Sea-salt vertical profiles over the Southern and tropical Pacific oceans: Microphysics, optical properties, spatial variability, and variations with wind speed

Yohei Shinozuka, Antony D. Clarke, Steven G. Howell, Vladimir N. Kapustin, and Barry J. Huebert

Department of Oceanography, University of Hawaii at Manoa, Honolulu, Hawaii, USA

Received 1 May 2004; revised 17 August 2004; accepted 18 September 2004; published 16 December 2004.

[1] About 100 vertical profiles of marine aerosol were contrasted between two remote regions over the Southern Ocean and the equatorial Pacific. Real-time thermal analysis of particles at near 40°C, 150°C, and 300°C resolved the volatile (mostly sulfate and organic) and refractory (mostly sea salt) size distributions continuously throughout two major aircraft campaigns. The average sea-salt contributions to aerosol optical depths (AOD) in the marine boundary layer over the Southern Ocean and tropical Pacific were 0.037 (63% of the total column AOD) and 0.022 (31%), respectively, while the volatile component contributed 0.011 (19%) and 0.038 (53%), respectively. This shows the large difference in relative importance of sea salt and volatile components for regions with different residence times and source strengths. The total column AOD is estimated to be 0.037, 0.043, and 0.090 for 0–4, 4–8, and 8–12 m s^{-1}, respectively, over the Southern Ocean, and 0.060, 0.062, and 0.128 for 3–5, 5–7, and 7–9 m s^{-1}, respectively, over the tropical Pacific. Wind speed was a good indicator of sea-salt concentrations on a campaign average basis but a poor indicator on a case-by-case basis. This highlights the important effect of removal, wind duration, and fetch on sea-salt variability. Variability in the marine aerosol was assessed statistically for 96 circular flight legs of about 60 km diameter. This mesoscale variability increased with altitude and resulted in variations in column AOD of about 25% over these spatial scales. Hence mesoscale variability is an important concern for satellite remote sensing, closure studies, and model validation even for this nominally homogeneous clean marine atmosphere. *INDEX TERMS:* 0305 Atmospheric Composition and Structure: Aerosols and particles (0345, 4801); 0365 Atmospheric Composition and Structure: Troposphere—composition and chemistry; 0394 Atmospheric Composition and Structure: Instruments and techniques; 0368 Atmospheric Composition and Structure: Troposphere—constituent transport and chemistry; *KEYWORDS:* sea salt, light scattering, vertical profiles

Citation: Shinozuka, Y., A. D. Clarke, S. G. Howell, V. N. Kapustin, and B. J. Huebert (2004), Sea-salt vertical profiles over the Southern and tropical Pacific oceans: Microphysics, optical properties, spatial variability, and variations with wind speed, *J. Geophys. Res.*, *109*, D24201, doi:10.1029/2004JD004975.

1. Introduction

[2] Aerosols in the remote marine boundary layer (MBL) are often dominated by two major species, sea salt and sulfate, with a smaller and poorly characterized fraction of organic aerosols and occasional dust. Sea-salt particles are generated in the atmosphere by wind-induced wave breaking and bubble bursting (see *Andreas* [1998] for a review and *Blanchard and Woodcock* [1957]). The number of non-sea-salt sulfate particles is often controlled by the subsidence from the free troposphere [*Bates et al.*, 1998b, 2001; *Clarke et al.*, 1996, 1998b; *Koponen et al.*, 2002] and less frequently by local nucleation process [*Clarke et al.*, 1998a; *Covert et al.*, 1992; *Hegg et al.*, 1992; *O'Dowd et al.*, 2002; *Pirjola et al.*, 2000; *Weber et al.*, 1998, 2001], linked to emissions of gaseous dimethylsulfide (DMS) produced by phytoplankton in the ocean surface. Owing to their ubiquitous presence over approximately 70% of the Earth's surface, the marine aerosols can play important roles in the global climate and atmospheric chemistry. Larger sizes dominate scattering of short-wave radiation that directly affects the Earth's radiation budget and lowers visibility over the ocean. Smaller sizes with a threshold diameter above about 0.08 μm can serve as natural cloud condensation nuclei (CCN) [*Charlson et al.*, 1987; *Hoppel et al.*, 1990; *O'Dowd and Smith*, 1993].

[3] Wind speed influences the production, transport and removal of marine aerosols. Many early studies associate variation in particle concentrations with wind-related turbulence at the air-sea interface [*Lovett*, 1978; *Nilsson et*

0148-0227/04/2004JD004975$09.00

al., 2001; *O'Dowd and Smith*, 1993; *Woodcock*, 1953]. Observations with robust statistics, however, have not found a clear dependency, presumably because concentrations reflect size-dependent production and removal during typical aerosol residence times. For example, *Bates et al.* [1998b] found that the wind speed accounts for no more than one third of the variance in the near-surface coarse-mode particle concentration measured from the R/V *Discoverer* over the Southern Ocean. We will take advantage of our extensive aircraft measurements to examine this issue further here in a three-dimensional context.

[4] The natural marine aerosol affects the global radiation budget. Sea salt may contribute more than half of the near-surface light extinction even near regions influenced by biomass burning [*Quinn and Coffman*, 1999; *Quinn et al.*, 2001]. The estimated contribution of the marine aerosol to aerosol optical depth (AOD) in visible wavelengths or the extinction coefficient integrated over the vertical column varies between 35 and 80% depending on the geographical location [*Quinn et al.*, 2001]. Because of this significance, the generation and vertical distribution of marine aerosol need to be better characterized in the context of regional meteorological features.

[5] Patchiness in the aerosol distribution can influence the strategy for sampling a region such as the number, length and type of sample legs. A reliable assessment of spatial variability is important if one requires representative data with a limited number of flight hours. It is also a source of uncertainties for column closure, or comparison of similar column measurements from different instruments based on one or more platforms such as aircraft, satellites and ground stations [*Redemann et al.*, 2003]. This variability will constrain spatial scales over which the measured aerosol optical properties should be averaged and those for obtaining representative profiles designed to address column properties.

[6] In this paper we describe the vertical profile of the marine aerosol size distribution and the associated light scattering characteristics along with their variations with wind speed. We use observations made aboard aircraft during the First Aerosol Characterization Experiment (ACE 1) [*Bates et al.*, 1998a] and the Pacific Exploratory Mission Tropics B (PEMT-B) [*Fuelberg et al.*, 2001], because the clean marine air masses encountered during these two major campaigns are affected by a minimum amount of dust and anthropogenic aerosols. Before we describe aerosol properties under ambient conditions, we examine the consistency and uncertainty associated with these airborne measurements. This includes various adjustments to sampled dry aerosol distributions that are required for translating aircraft measurements subject to humidity changes and sampling losses, etc. to ambient aerosol properties. These are based upon our size-resolved knowledge of aerosol properties and aircraft sampling performance. During this process we will confirm that resulting aerosol properties are consistent with independent measurements of these properties through so-called "closure" exercises [*Redemann et al.*, 2003] including a discussion of associated uncertainties. These are not only important for evaluation of our subsequent measurements and modeling, but also helps identify factors that limit our understanding of the aerosol characteristics. We will finish with an examination of the spatial variability of marine aerosol and its significance.

2. Measurements and Data Validation

2.1. Aircraft Experiments

[7] Two aircraft campaigns in the marine boundary layers over the extensive regions of the remote Southern and Pacific Oceans provide the data for this study. ACE 1 employed the National Center for Atmospheric Research C-130 aircraft to measure microphysical, chemical, and optical properties of tropospheric aerosols over the southwest Pacific Ocean, south of Australia (Figure 1) in November and December 1995 [*Bates et al.*, 1998a]. About 60 hours were spent in the lowest 2000-m layer over the open ocean during 18 flights. These flights included about 70 column profiles to obtain the vertical structure of the aerosol properties and many horizontal legs, each of which lasted typically for 30 min over a circle of 60 km in diameter.

[8] PEMT-B employed the National Aeronautics and Space Administration P-3B aircraft to fly over the tropical Pacific Ocean (Figure 1) in March and April 1999 [*Fuelberg et al.*, 2001]. About 50 hours was spent in the lowest 2000-m layer over the open ocean during 15 flights. For both experiments some of the data were associated with pollution, indicated by high number ratio of heated (residual) to unheated (total) particles measured with condensation nuclei counters [*Clarke et al.*, 2001]. Also, some data were associated with cloud and rain events, indicated by high (>95%) ambient relative humidity (RH). These data represented 7% of the whole data set and were removed from the analysis for this study.

2.2. Size Distribution Measurement

[9] Here we emphasize the size distributions measured behind the aircraft inlets under dry conditions. We take into account the recognized effects of size-dependent sampling losses in the aircraft inlet and RH growth through comparisons to independent measurements as described below. The relevant instruments are briefly described here and detailed elsewhere [*Clarke et al.*, 1998b].

[10] A laser optical particle counter (OPC) (Particle Measurement Systems LAS-X, Boulder, Colorado modified for 256 channel resolution) measured the number size distribution over optically effective diameters of 0.15–7.7 μm under dry conditions (RH $\sim$ 20% after mixing with equal parts of desiccated air). The inlet temperature was controlled to near 40°C, 150°C and 300°C to infer aerosol composition from volatility [*Clarke*, 1991]. A sequential cycle through these three temperatures took 2–3 min. The OPC sized individual particles based on the scattering-to-size relationship established for polystyrene latex spheres (PSL) (refractive index n = 1.59) and glass beads (n = 1.54). This sizing procedure assumed measured particles to have similar refractive indices to those of the calibration particles, and worked fine for dry sea salt ($n \sim 1.57$). However, refractive indices of the unheated particles in the accumulation mode (e.g., sulfate) were estimated to be smaller ($n \sim 1.47$), and optically effective diameters were deter-

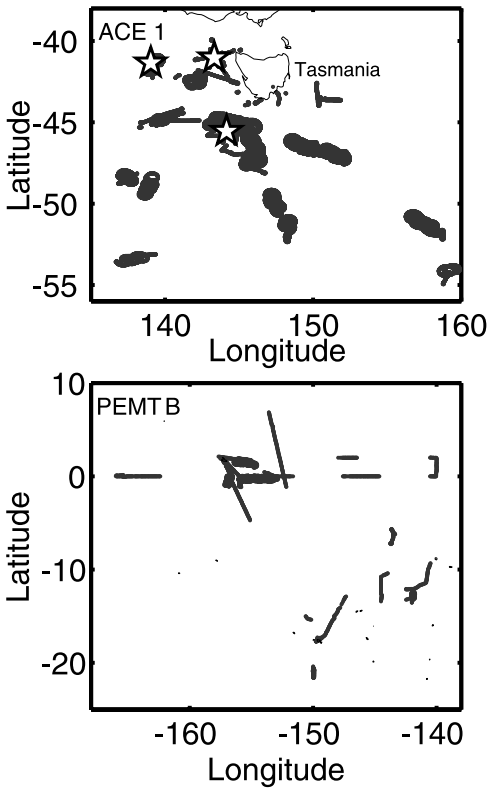

Figure 1. Aircraft tracks in the lowest 2000-m layer during the (top) First Aerosol Characterization Experiment (ACE 1) and (bottom) Pacific Exploratory Mission Tropics B (PEMT-B). For ACE 1 the three ship locations for the Sun photometer measurements are indicated by white stars.

mined accordingly. These were calculated from the difference in OPC response for the calibration and measured particles, which in turn was computed for their refractive indices, the OPC detection angle (35°–145°) and the wavelength (633 nm) based on Mie theory [*Pinnick et al.*, 2000].

[11] The OPC measured particles behind the Community Aerosol Inlet (CAI) during ACE 1 and Solid Diffuser Inlet (SDI) during PEMT-B, where large particles later found depleted via collision with the inner wall. In order to relate the OPC size distributions to ambient distributions, they were divided by the appropriate transmission efficiency for each inlet. The transmission efficiencies have recently been made available as a result of intercomparison of the CAI, SDI, and Low Turbulence Inlet (LTI) during the aircraft campaign after ACE 1 and PEMT-B, Passing Efficiency of the Low-Turbulence Inlet (PELTI) [*Huebert et al.*, 2004]. However, dust particles were sampled in addition to sea-salt particles at low altitudes during PELTI, while most of the coarse-mode particles were dominated by sea salt during the other two campaigns. Dust particles observed during PELTI may bounce on the inner wall of CAI and SDI more readily than sea-salt particles, which may justify smaller efficiencies than what are used here. In addition the LTI enhancement calculation (upon which the CAI and SDI efficiency estimates are based) may increase the uncertainty in the resulting inlet efficiencies. Nonetheless, the PELTI intercomparison provides the best available estimate of the CAI and SDI transmission efficiencies and through closure tests we demonstrate that they yield representative ambient size distributions.

[12] Transmission efficiencies are size-dependent and lower for larger particles. The 50% size cut was found to be at 2.1 um and 8.4 μm in dry aerodynamic diameter for the CAI and SDI, respectively. For each inlet, the degree of uncertainty was inferred from the variances in the six comparisons made during the PELTI experiment. This poses the largest uncertainty in mass estimates that are dominated by larger sizes, as discussed in section 2.3. However, the recent DC-8 Inlet/Instrument Characterization Experiment (DIC) (2003) using the SDI showed that the inlet losses for integral scattering values were only on the order of 10% for both marine and dust environments (K. Moore, personal communication, 2003). Later we demonstrate that calculated OPC mass and measured external mass generally agrees well within these nominal uncertainties (section 2.3).

[13] The instruments inside the aircraft were deliberately operated under low RH to enable direct comparison between measurements and to reduce uncertainties from the effect of humidity on particle size and composition. Consequently, in order to reconstruct the aerosol size distributions under ambient RH, typical diameter adjustments are required. The diameter growth factor, g(RH), was calculated for sodium chloride after *Tang* [1997]. This growth factor is 1.6 for 60% RH and 1.9 for 80% RH relative to the OPC RH of 20%. For the 40°C and 150°C distributions in the accumulation mode we used volume-weighted average of the ammonium sulfate [*Potukuchi and Wexler*, 1995] and the sea-salt growth factors, which took 1.3 for 60% RH and 1.6 for 80% RH. The particle diameters under the ambient conditions were generated from products of the OPC diameters and the RH-dependent growth factor.

2.3. Size Distribution Validation

2.3.1. Local Optical Closure

[14] In order to confirm that the measured dry OPC size distributions were representative, we evaluated "closure" with integral light scattering also measured inside the aircraft. The dry aerosol scattering coefficient (~25% RH) was measured at 450, 550, and 700 nm every 15 s with an integrating nephelometer (TSI, Model 3563) [*Anderson et al.*, 1996] with a precision of 0.1 Mm^{-1} over a 1-min period. An impactor with a cutoff aerodynamic diameter of 1.0 μm was inserted periodically into the flow to obtain the scattering coefficient of submicron particles. In order to avoid having mixed aerosol distributions in the nephelometer, data were removed for the 40 s following each impactor switch. The nephelometer measurements were compared with scattering derived from size distributions using Mie theory for three other input parameters: (1) the nephelometer wavelengths, (2) the nephelometer detection angle range of 7°–170°, and (3) the refractive indices estimated for dry particles as mentioned above.

[15] Each data point in Figure 2 represents average OPC and nephelometer scattering coefficients at the instrument pressure during a horizontal leg that lasted for 20 min or longer. One data point was removed because the leg was

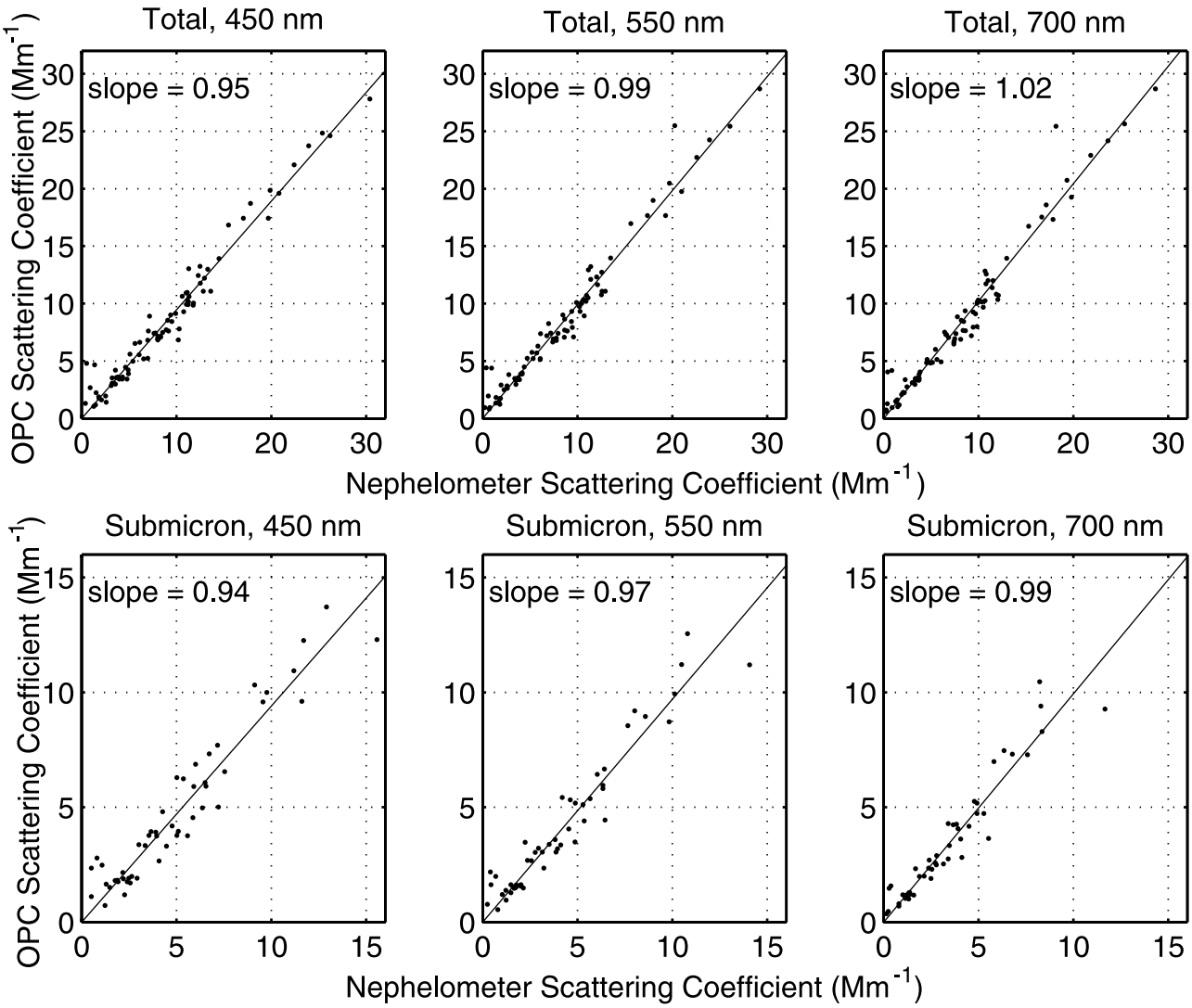

Figure 2. Scattering closure between the optical particle counter (OPC) and nephelometer airborne aerosol measurements under the low relative humidity during ACE 1. Each dot represents average values over a horizontal leg that lasted for >20 min in the remote marine air. Slopes of the regression lines are also indicated. (top) Total aerosol. (bottom) Submicrometer aerosol.

flown through a large scattering gradient over an inversion at 1400 m. We also note that the two instruments, as well as the internal mass sampler described later, observed particles up to the same size, because all of them were located behind the inlet that rarely passed particles larger than 9 μm in aerodynamic diameter [*Blomquist et al.*, 2001]. The resulting comparison at 550 and 700 nm have slopes close to 1:1. This demonstrates local closure for total and submicron particles and indicates that our OPC measurements and refractive index assumptions reliably reflect the actual microphysical, chemical and optical properties of the particles sampled through the inlet. The scattering measurement at 450 nm tends to have a smaller signal-to-noise ratio and results in the larger differences between the OPC and nephelometer data.

2.3.2. Internal Mass Closure

[16] As a further test of optical and mass closure, the 300°C OPC volume distribution was converted to dry mass and compared with an independent measurement of dry sea-salt mass. Chloride and sodium were regularly collected on filters inside of the aircraft [*Huebert et al.*, 1990; *Huebert et al.*, 1998] during ACE 1 and analyzed after the flights for individual or multiple sample legs. This internal sampler required integration times of 30 min or longer. After ion chromatography analysis, the sea-salt mass was obtained as the weight sum of chloride and 1.47 times sodium as suggested by *Quinn et al.* [2001]. To yield a comparable mass to that collected by the sampler, the heated OPC distribution was averaged over each time period when the internal sampler was operated, multiplied by the sampler transmission efficiency [*Blomquist et al.*, 2001, Figure 6], integrated over size, and multiplied by the dry sea-salt density of 2.2 g cm^{-3}. The solid dots in Figure 3 show the resulting internal mass comparison. About half of data have error bars that include the 1:1 line (solid line), while the linear regression (dashed line) suggests a possible overestimate of the OPC-derived mass by about 20%. A density of 1.8 g cm^{-3} would result in a good agreement.

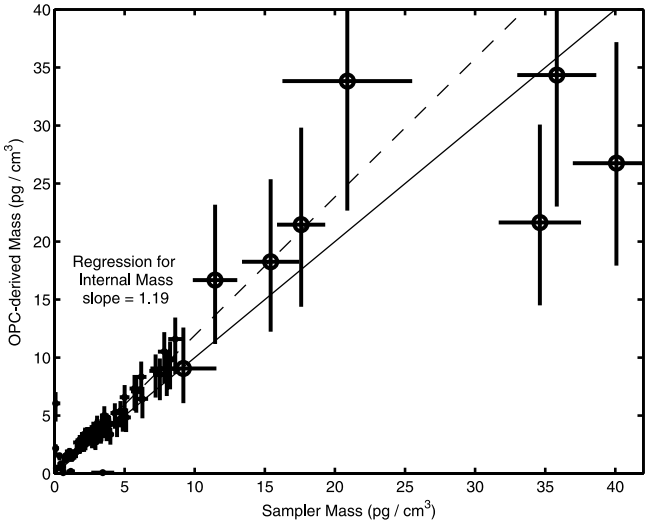

Figure 3. Dry sea-salt mass comparison between the OPC and the filter samplers inside (dots) and outside (circles) the aircraft during ACE 1. The dashed line shows the linear regression for the internal mass comparison. For the OPC-derived mass calculation the dry sea-salt density of 2.2 g cm^{-3} was applied to the size distributions at 300°C averaged over ~30 min. For the external comparison the OPC size distributions were corrected for the inlet loss.

[17] This overestimate may be due to error in our density estimate or diameter adjustment. It is not likely that the OPC sample line caused additional loss, because its derived scattering coefficients agree nicely with the nephelometer measurements. The density may be overestimated by the assumption that the sea-salt particles were completely dried out at 300°C OPC measurements. Through gravimetric and ion chromatography analysis with submicrometer remote marine sea-salt aerosols, *McInnes et al.* [1994] found that 26 ± 5% in mass remains bound to sea salt when RH was decreased to 40% and that the crystallization humidity lies below 9% RH. We speculate that bound water up to 20% in mass can remain in sea-salt particles at the OPC RH of about 20%. They also state that virtually no water was associated with sea-salt particles after heating them at 110°C overnight. It is uncertain if the particle residence time in our OPC 300°C scans, ~1 s, is long enough to dry them out (while it is certainly long enough for water coatings or externally mixed volatile components to be evaporated). Bound water could make the dehydrated sea-salt mass smaller by up to 20%, although this effect is counteracted by larger diameter adjustment due to the smaller refractive index that would shift diameter to larger side by several percent. Alternatively, the OPC overestimate may be caused by the spherical particle assumption. The light scattering due to aspherical particles over the super-micron diameter range is generally larger than what Mie theory predicts for the equivalent-surface-sphere spherical particles [*Mishchenko et al.*, 1997] but is expected to be small for sea salt. The resulting OPC size would be larger than the actual surface-equivalent size, thereby making the derived-mass larger than the real mass. Also, the sample mass could be underestimated because of variable volatility of chloride.

2.3.3. External Mass Closure

[18] Application of the inlet transmission efficiencies to the measured dry size distributions yield the effective dry ambient size distribution. This can be integrated over size to test for closure with the sea-salt mass measured in the total aerosol sampler (TAS) mounted outside the aircraft [*Huebert et al.*, 1990; *Huebert et al.*, 1998]. The eight open circles in Figure 3 compare the OPC-derived dry ambient sea-salt mass with the dry sea-salt mass obtained from the external sampler during ACE 1. The sampler specification is the same as the internal filter sampler mentioned above except for more limitations in sample number and available chemical species. The OPC mass was derived from the average distribution at 300°C in each of the horizontal legs when the external sampler was operational (once per flight). The filter sea-salt mass is given here as 3.27 times the sodium weight since chloride weight was not available. Most of the error bars include the 1:1 line, and most of the external sampler mass versus OPC-derived mass exhibit a relationship consistent with that for the internal sampler. This general agreement for both internal and external samplers supports our interpretation of CAI performance during ACE 1. We note that coarse dust might be mistaken for refractory salt by the OPC. However, dust should not be correlated with sea salt and should randomly affect the variability on OPC derived mass. The reasonable fit shown in Figure 3 suggests that any contributions to refractory mass from dust must lie within the error bars of the OPC measurements, supporting our assumption of negligible dust presence. The underestimate of the OPC-derived mass evident for cases of highest mass is partly attributed to particles larger than about 4 μm in dry diameters that were collected on the external filter but have the largest uncertainty in their CAI transmission efficiency. Again, we note that optical scattering will be far less sensitive than mass to uncertainties in large particle transmission efficiency.

2.3.4. Column Aerosol Optical Depth Closure

[19] An overall evaluation of the OPC measurements and adjustments including the RH growth was possible for several cases when the aircraft made descent profiles near the National Oceanic and Atmospheric Administration R/V *Discoverer* during ACE 1. These allowed direct comparison of our differential column AOD derived from our ambient size distributions with AOD measured aboard the ship at 500 and 778 nm with a hand-held Sun photometer. The random uncertainty in the Sun photometer measurement is estimated to be ±15% (P. K. Quinn, personal communication, 2002).

[20] During Flight 17, 22 and 24 the column optical depth was measured within 1° latitude and longitude of profiles made on the C-130. To obtain effective column AOD to be compared with these shipboard measurements, individual contributions to AOD due to aerosols over 0–2000 m, 2000–5500 m and 5500 m-top of atmosphere were separately estimated for the three time periods. The differential AOD over the altitudes up to 2000 m were given as integral of the OPC-derived wet ambient scattering coefficients computed at the Sun photometer wavelengths of 500 and 778 nm. A linear interpolation was made from scattering coefficients measured at adjacent altitudes for the few

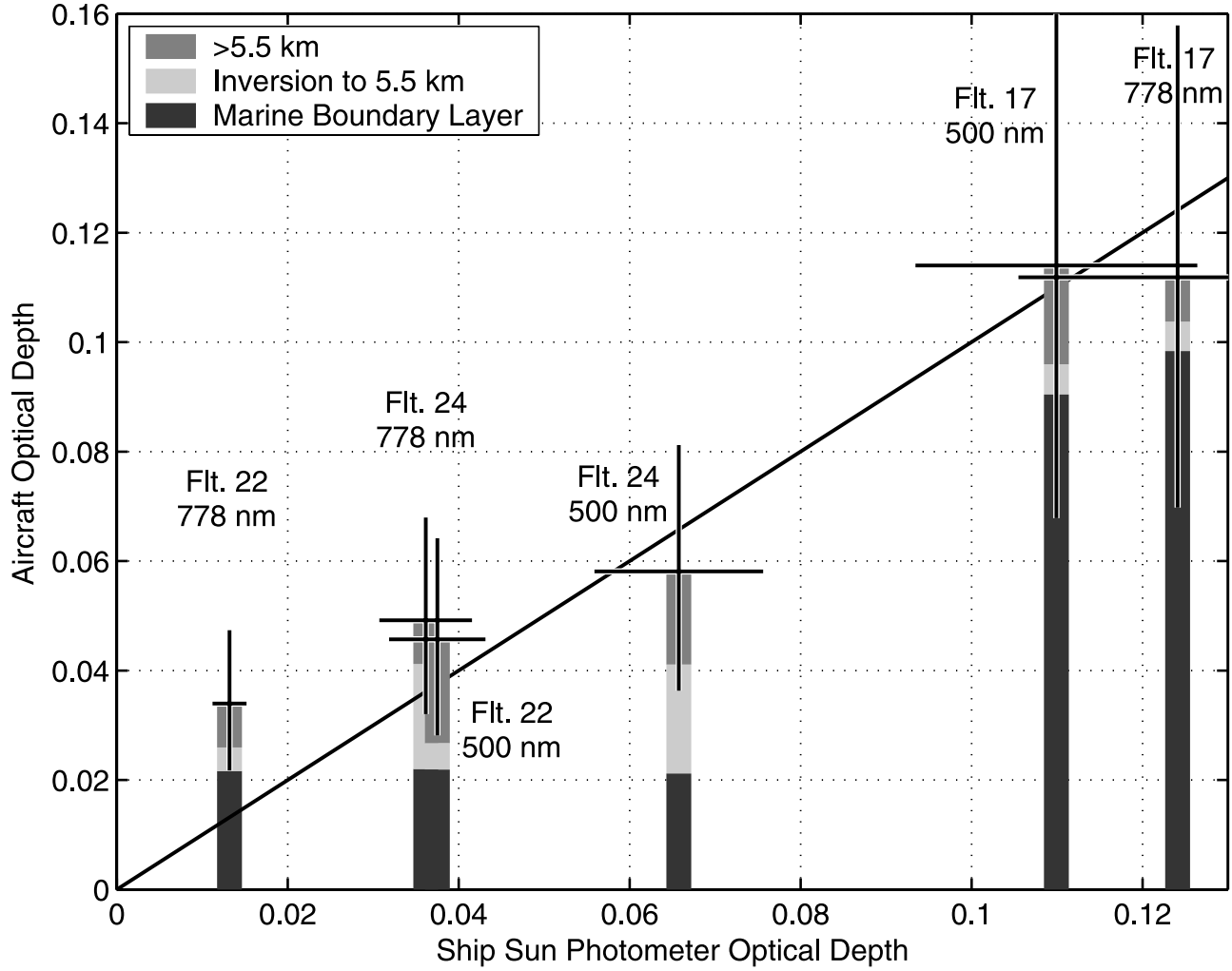

Figure 4. Aerosol optical depth comparison between the Sun photometer measurements aboard R/V *Discoverer* and estimate based on the C-130 measurements and SAGE II observation.

altitudes that lacked an OPC measurement. The differential AOD between 2000 and 5500 m were derived from the nephelometer scattering coefficients through the same interpolation and integration processes. For the differential AOD between 5500 m and top of atmosphere we used *Fridlind and Jacobson*'s [2003] values. They scaled the SAGE II measurements at 525 nm to obtain the differential AODs at 500 and 778 nm using the wavelength dependency of the AOD inferred from the Mie calculation for the free troposphere aerosols. These are the closest data for contributions above 5500 m that were available but may not always be representative of where we flew.

[21] The result is shown in Figure 4. The column optical depths derived from the aircraft measurement agree with the direct measurements within differences ranging from −0.004 to +0.022 (−6 to +32%). We note that the ship optical depth during flight 17 was measured only once per each of the Sun photometer wavelengths. The other two points should be given more weight because they are averages of 9 (Flight 22, 8 for the 778 nm measurement) and 2 (Flight 24) independent Sun photometer measurements. Also, a bias to higher values can be expected in shipboard Sun photometer measurements because of subvisible cirrus in the region as well as difficulty in aligning the instrument with the sun on a moving platform [*Porter et al.*, 2001]. From the flight 22 measurements we removed three data points from the ship AOD measurements before averaging, because they are either extremely large or small relative to the other data points (they are 3.5, 5.7 and 0.05 times as large as the average). We consider the AOD agreement between the in situ and ship measurements very good as it falls within the typical spatial variability discussed in section 4. This agreement implies that the OPC measurement as well as our refractive index, inlet efficiency and RH growth are consistent within the identified uncertainty and can be used more generally in AOD assessments during other ACE 1 profiles.

2.3.5. Uncertainty

[22] Nominal uncertainties associated with the derived OPC scattering and mass were taken as the square root of sum of square of uncertainties in the OPC measurement and above mentioned assumptions, as detailed in Table 1. Our OPC calibration is estimated to have a 5% uncertainty in sizing due to the small sensitivity of scattering intensity to the particle size. In addition, *Reid et al.* [2003] recognize particle nonsphericity and refractive index as possible

Table 1. Uncertainty in the Scattering and Mass Calculated From the Optical Particle Counter Distributions[a]

Factors		Scattering, %	Mass, %
	Measurements		
a	Measurement (total of a1 and a2)	+16/−14	±15
a1	Flow rate and counting	±3	±3
a2	Calibration, ±5% associated with diameters	+16/−14	±15
b	Refractive index estimate for diameter adjustment	+6/−5	0
c	Inlet transmission efficiency estimate[b]	+26/−13	+36/−20
d	RH adjustment (total of d1 and d2)	+6/−20	+8/−28
d1	Growth factor, +0/−10%[c]	+0/−19	+0/−27
d2	RH measurement, ±3%	±6	±8
e	Density for converting volume to mass	0	+0/−20
	Environmental Factors		
f	Mesoscale variability[d]	±23	
g	FT scattering coefficient	+14/−8	
h	Stratosphere differential AOD estimate[e]	±25 (500 nm), ±15 (778 nm)	
	Resulting Products		
	Dry aircraft scattering coefficient (total of a and b)	+17/−15	
	Internal mass (total of a, b, and e)		+15/−25
	External mass (total of a, b, c, and e)		+39/−32
	Wet ambient scattering coefficient (total of a–d)	+32/−28	
	Column AOD (total of a–d and f–h)	+49/−45 (500 nm), +44/−40 (778 nm)	

[a]AOD, aerosol optical depths; FT, free troposphere; and RH, relative humidity.
[b]Estimated from the variance during the PELTI experiment [*Huebert et al.*, 2004], and is dependent on particle size. The resulting uncertainties in scattering and mass are given as its integral over the observed size distribution.
[c]Estimated for the ranges of growth factors suggested by *Tang et al.* [1997] and *Swietlicki et al.* [2000].
[d]Estimated from vertical integral of mean coefficient of variance in the ambient scattering coefficients for horizontal legs >20 min.
[e]Estimated from the range of the integrated uncertainties reported with the SAGE II data at each wavelength [*Fridlind and Jacobson*, 2003].

factors for oversizing of dust particles with their forward scattering spectrometer probe. Nonspherical particles tend to scatter more in the side angles than spherical particles of the same surface-area-equivalent diameter [*Mishchenko et al.*, 1997], thereby enhancing our OPC response. The dry sea-salt nonsphericity is much smaller than that of the dust and should result in negligible oversizing [*Kalashnikova and Sokolik*, 2002]. The real refractive index for dry sea salt is close to that of the calibration particles and therefore not a source of significant OPC sizing uncertainty. As a result, our OPC dry scattering coefficient estimate is primarily affected by the choice of submicron volatile particle refractive index. However, the high correlations shown in Figure 1 confirm that this is not large.

[23] The dry sea-salt mass estimates are uncertain due in part to our dry sea-salt density uncertainty (0–20%) and the OPC measurement uncertainty. The inlet passing efficiency explains most of the uncertainty in the calculated external mass, and is also a considerable source of uncertainty in the external scattering. The ambient scattering was calculated to be about 2.8 times as large as the measured dry scattering and had an uncertainty of 30% based on the ranges of growth factors suggested by *Tang et al.* [1997] and *Swietlicki et al.* [2000].

[24] The procedures used above demonstrate that we have closure between our OPC size distributions and measured aerosol optics and mass both inside and outside the aircraft except over the largest size range. A possible large particle deficit can be estimated from comparison to previous measurements. *Woodcock* [1953] observed coarse sea-salt particles collected on glass slides from a small aircraft exposed to the ambient air near cloud bottom, 500–800 m above sea level. On the basis of this observation, *Porter and Clarke* [1997] parameterized sea-salt size distributions for 12 wind speed categories. Both OPC-derived and Woodcock's number distributions are converted to scattering distributions using Mie theory with a refractive index of 1.57 at 550 nm. As shown in Figure 5, the OPC-derived distribution underestimates dry ambient scattering for >4 μm compared to Woodcock's observation. The differences in scattering for the large diameters are 15% and 25% of the total modeled scattering for the local wind speed ranges of 5.5–7.9 m s^{-1} and 13.9–17.1 m s^{-1}, respectively. The differences in mass are 100% or larger, but the rapid decrease in the mass scattering efficiency with size makes the underestimate in scattering coefficient much smaller. Woodcock's data are based on small number of samples taken under a limited variety of meteorological conditions, so large deviations may exist relative to actual ambient sea-salt distributions during ACE 1. Hence, given the range of real variability present (see section 4) and the differences in measurement conditions and sampling approaches, we consider these differences to be within expected variability.

3. Ambient Size Distribution, Vertical Scattering Profile and Optical Depth

3.1. Number and Volume of Marine Aerosol Components

[25] In order to study the aerosol optical properties we start with the size distributions and their chemical composition inferred from their volatility. Here we describe the sea salt and volatile differential AOD separately for accumulation and coarse modes along with their variations with wind

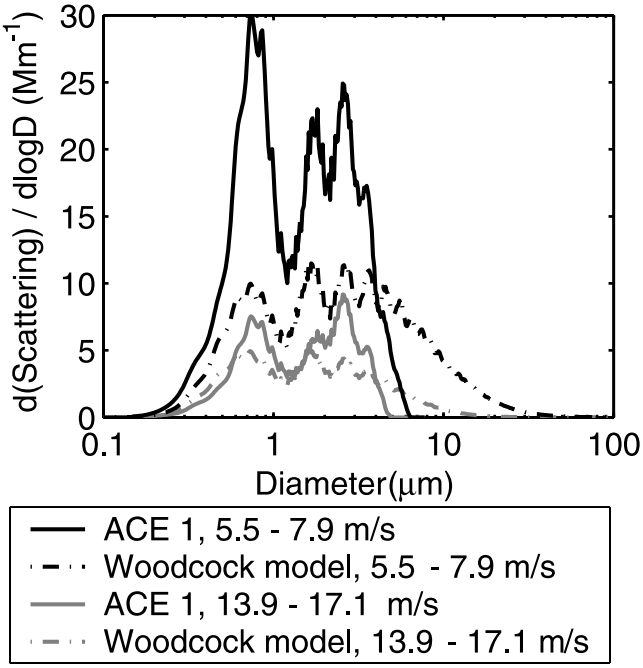

Figure 5. The OPC-derived and model [*Porter and Clarke*, 1997] dry ambient scattering distributions for two local wind speed categories, 5.5–7.9 m s^{-1} and 13.9–17.1 m s^{-1}. The model distribution in the large end is based on *Woodcock*'s [1953] observation made at cloud bottom, 500–800 m above sea level near Hawaii. The OPC-derived distributions are averages of ACE 1 measurements over the same altitude range over the open ocean under the same local wind speed ranges.

speed. We first characterize observations in the lowest 200-m altitude bin. These results are then extended into discussions of their vertical gradient. We note that although we demonstrated the mass closure for most data (Figure 3), the measured size distributions are not intended to quantify the total aerosol mass loading. Our primary objective is to assess size-dependent scattering due to each component. This scattering is typically better constrained than the mass because it has only a small contribution from the mass in larger sea-salt sizes because of their much lower mass scattering efficiency.

[26] The ACE 1 ambient size distributions were categorized into three wind speed categories, i.e., 0–4, 4–8 and 8–12 m s^{-1} based on average 10-m wind speed. The 10-m wind speed was estimated from the wind speed measured at aircraft altitudes over the time period between 2 hours before and after a given measurement under an assumption of logarithmic increase with height [*Paulson*, 1970]. For this estimate, surface roughness height was calculated using drag coefficient given by *Large and Pond* [1981] and the Charnock constant [*Wu*, 1982]. Compared to average wind speed measured over 30–200 m, the scaled 10-m wind speed is smaller by 15–25%. This wind speed computation method is generally valid for a neutrally stable surface layer but also appeared to be consistent with ACE 1 data. During one of the ACE 1 ship-aircraft intercomparison, the mean wind speed was measured as 12.3 m s^{-1} at 30 m high on the R/V *Discoverer* and agreed within 0.3 m s^{-1} of the mean 30-m wind speed computed from the aircraft observations during horizontal legs at 160 and 60 m flown within 1° of longitude and latitude of the ship location. In the tropics during PEMT-B the 10-m wind speed encompassed a narrower range of values so the size distributions are categorized into 3–5, 5–7 and 7–9 m s^{-1}.

[27] The integrated number, volume and scattering coefficient are binned into these wind regimes for the entire ACE 1 (Figure 6) and PEMT-B (Figure 7) experiments. Within each regime there is little difference in the coarse particle volume among the three OPC temperatures, i.e., 40°C, 150°C and 300°C, as expected for refractory sea salt. In contrast, particle sizes between 0.15 and 1 μm show large difference between the 40°C and 300°C. Most of the particles in this size range are volatile, as expected for sulfate and some organic aerosols. However, refractory sea salt still contributes 10–30% of the submicrometer particle number (depending on altitude) when averaged over the all wind speed conditions and increases with wind speed in similar proportions as the coarse sizes.

[28] The average concentration of supermicron sea-salt particles is seen to be a strong function of wind speed. For example, in the lowest 200-m altitude bin the average refractory particle volumes for the wind speed ranges of 4–8 and 8–12 m s^{-1} are 4 and 7 times, respectively, as large as that under 0–4 m s^{-1}. This average behavior is consistent with wind-driven sea-salt production [*Blanchard and Woodcock*, 1980; *Twomey*, 1977]. We note that the fetch, wind variability, vertical mixing and removal processes, etc. are also important factors that determine the aerosol loading.

[29] The concentrations of submicron volatile particles (40°C minus 300°C data) with wind speed (Figure 6 right) remain in the narrow range of 19–32 cm^{-3} for all wind speeds and do not show a strong wind speed dependency (e.g., 25, 32 and 30 cm^{-3} for 0–4, 4–8 and 8–12 m s^{-1} over 0–200 m). Moreover, the number of smaller particles in 0.01–0.15 μm counted with a differential mobility analyzer (DMA) (data not shown) generally decreases with increasing wind speed by more than 50% (605 cm^{-3} for 0–4 m s^{-1} and 290 cm^{-3} for 8–12 m s^{-1}) over 0–200 m. Although we did not use a heater before the DMA to measure the volatile particle number, most of the Aitken particles are expected to be volatile judging from the low sea-salt fraction in the number distribution present over the smallest side of the OPC diameter range. These observations are consistent with an earlier ACE 1 paper where entrainment from the free troposphere is identified as an important particle source for those volatile aerosols [*Clarke et al.*, 1998b].

[30] A strong vertical gradient of supermicron sea-salt volume is evident in the average ACE 1 data (Figure 6 center). The coarse sea-salt volume at 600–1000 m altitude is 20–60% of that over 0–200 m for 10-m wind speed of 4–12 m s^{-1}. The accumulation mode volatile number gradient (Figure 6 left) shows less change with number concentrations in 600–1000 m about 60–90% of those in 0–200 m.

[31] In PEMT-B (Figure 7 center), the sea-salt volume for 0–200 m increases with wind speed in the same manner as in ACE 1, but the concentrations are about half as much. One distinctive characteristic of the PEMT-B accumulation

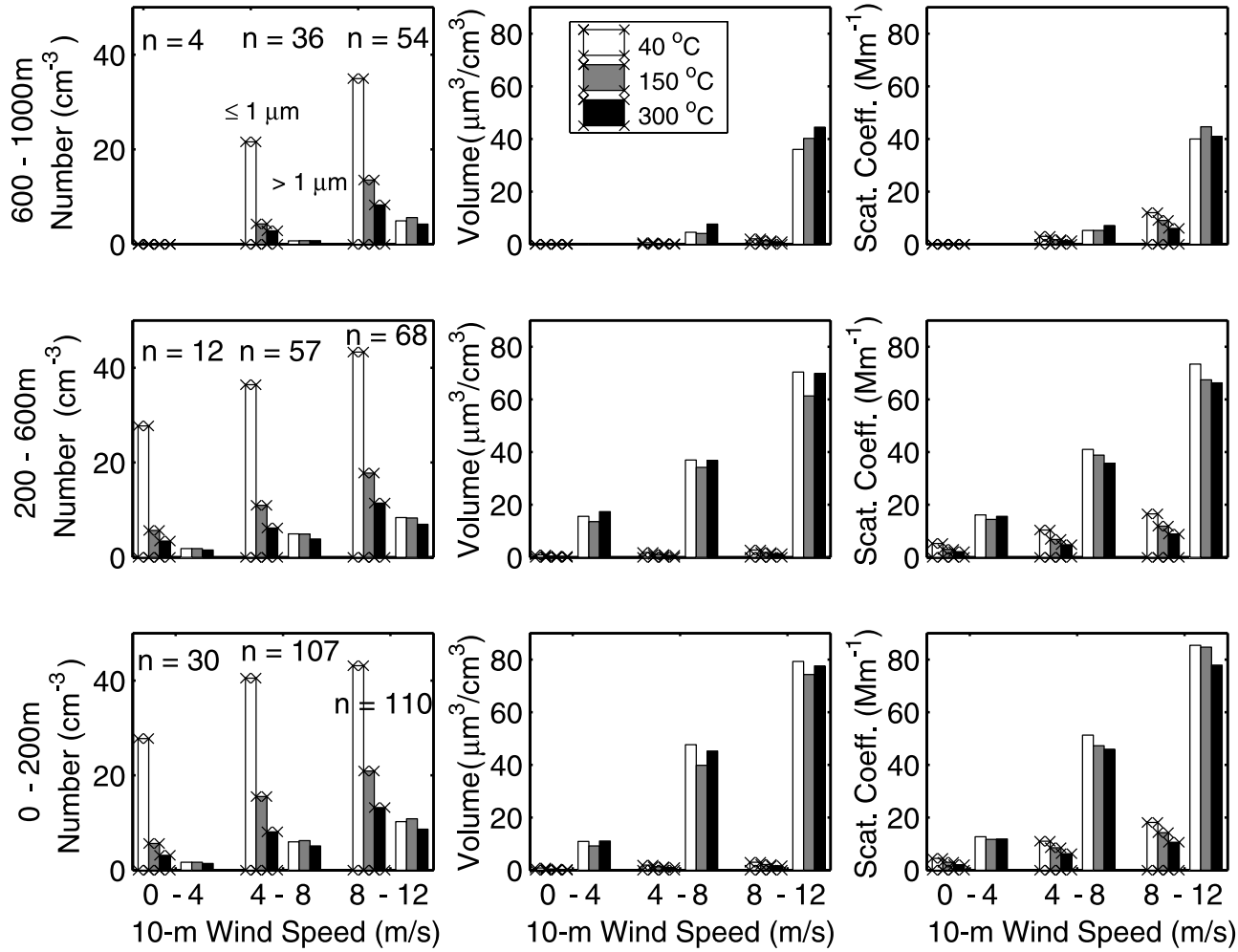

Figure 6. (left) Average number, (center) volume, and (right) scattering during ACE 1. White, gray and black bars represent OPC measurements at 40°C, 150°C, and 300°C, respectively, for submicron (three bars with crosses to the left) and supermicron (three bars to the right) particles under each altitude and 10-m wind speed category. Sample numbers are shown in the number graphs.

volatile particles is the smaller reduction in submicron particle number between 40°C and 150°C, indicative of a more neutralized aerosol [*Clarke*, 1991]. At least 90% of these particles appear neutralized in PEMT-B, while this fraction is rarely higher than 30% in ACE 1. The submicron refractory sea-salt number does not differ significantly between ACE 1 and PEMT-B, but the submicron volatile number for PEMT-B is 3–4 times as large as that for ACE 1. These differences may reflect the difference in sources, lifetimes and meteorology in these two regions, as discussed in section 5.

[32] These microphysical features are reflected in the associated light scattering (Figures 6 and 7 right). We will examine the average profiles of scattering due to sea salt and volatile particles with higher vertical resolution.

3.2. Average Scattering Coefficient and Its Wind Speed Dependency

[33] The ambient aerosol scattering coefficient and its column integral, or AOD, are of primary relevance to the aerosol direct effect on the Earth's radiative balance. It is important for observations and models to be capable of accurately representing their magnitudes and variations as well as the relative contributions due to different aerosol components. Here about 100 vertical profiles of scattering are examined to identify accumulation and coarse-modes contributions to extinction along with their vertical structures.

[34] Figures 8a–8d shows the ACE 1 vertical scattering profiles adjusted to ambient values based on our size distributions as described earlier for closure studies. Figures 8a–8c show the observations during legs where the 10-m wind speeds were 0–4, 4–8 and 8–12 m s^{-1}, respectively. All data are combined and plotted in Figure 8d. The open circles and solid circles in each plot indicate median values for ACE 1 over each 200-m altitude bin at 40°C and 300°C, respectively. It is important to note that the point-by-point variability (gray dots) at each altitude is real and consistently evident in both nephelometer data and the size distributions. The median ACE 1 values are then integrated over the column to obtain the indicated typical differential optical depths up to 1000 m (AOD_{1km}) and 2000 m (AOD_{2km}) at 500 nm wavelength. The scattering coefficient in the MBL decreases rapidly from the surface to about 1200 m due

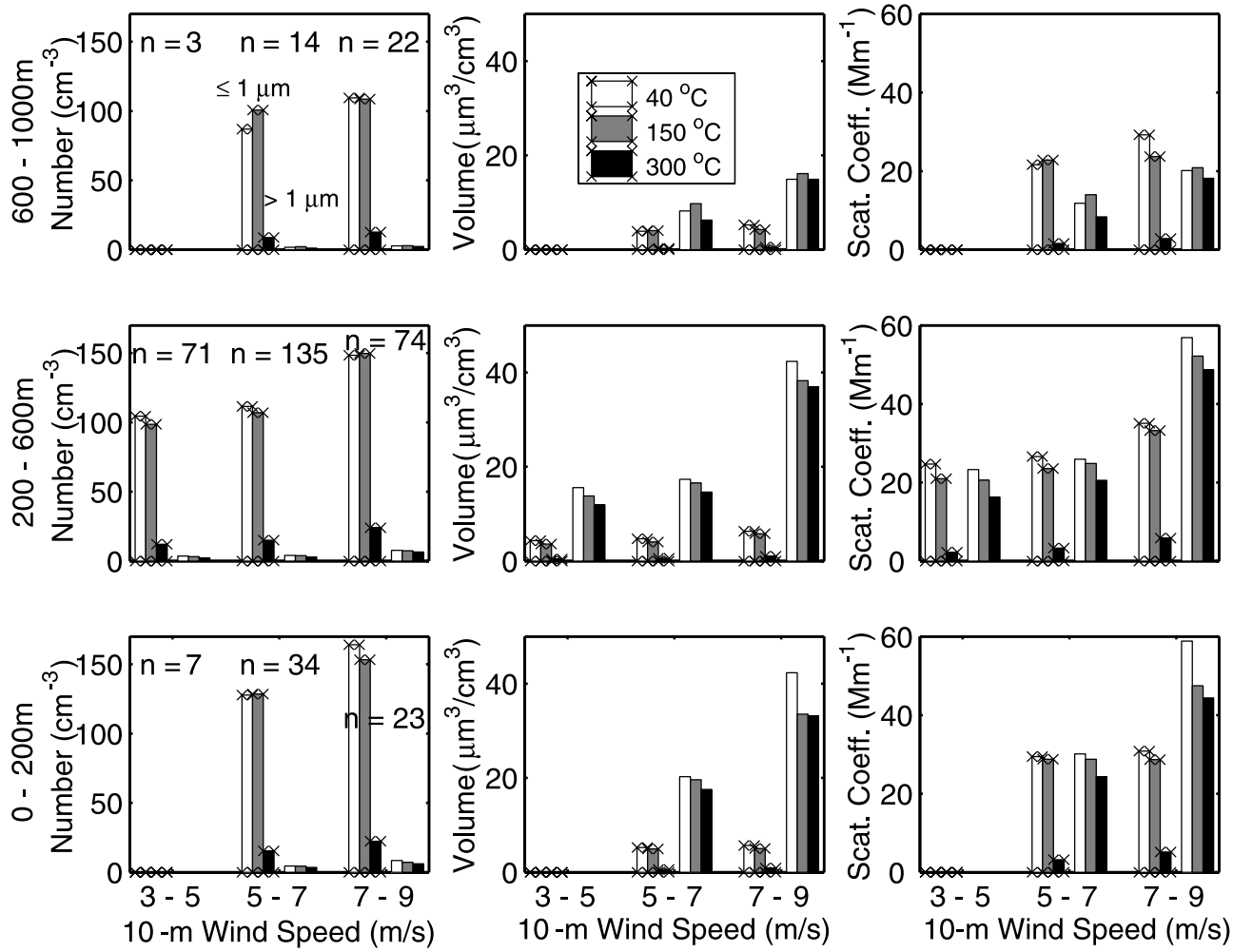

Figure 7. Same as Figure 6 except for PEMT-B and different scales.

mostly to the sea-salt vertical profile. This decrease in sea-salt aerosol concentration is very consistent with that presented by *Maring et al.* [2003]. The difference between 40°C and 300°C scattering coefficients is due to the volatile non-sea-salt components, and their contribution to scattering remains small in the MBL.

[35] The resulting average ACE 1 integrated differential AOD up to 1 km and 2 km is 0.041 and 0.048, respectively, for total particles and 0.035 and 0.037 for the sea-salt component for ACE 1. Note that these AOD values may have to be multiplied by a factor of 1.2 to account for the large particle sampling deficiency (Figure 5). Sea salt makes up 85% and 77% of the total scattering coefficients up to 1 km and 2 km, respectively. Similar evaluations for PEMT-B (not shown) revealed the average volatile and sea-salt AOD up to 2 km over the tropical Pacific Ocean to be 0.038 and 0.022, respectively, with the sea-salt contribution reduced to only 37%.

[36] The OPC-derived median ambient scattering coefficient up to 1200 m shows a general decrease with decreasing wind speed, as does the vertical gradient (Figures 8a–8c). The factor of 3–4 difference in average scattering between 0–4 m s^{-1} and 8–12 m s^{-1} is consistent with the well-known relationship between the wind speed and sea-salt generation [*Blanchard and Woodcock*, 1980; *Twomey*, 1977]. However, a large variance is evident in the ambient scattering coefficients in each wind speed category with values as small value as 15 Mm^{-1} or greater than 150 Mm^{-1} near the surface under 4–8 m s^{-1}. This clearly demonstrates that local wind speed alone is not capable of accurately predicting aerosol concentration and associated scattering properties on a case by case basis.

[37] The observations above are based on the OPC size distributions and thermal analysis. Unheated nephelometer measurements can also provide ambient scattering coefficient after adjusting for the nephelometer angular truncation [*Anderson et al.*, 1996] and scaling adjustments for the inlet loss and RH growth based on our size-resolved assessments, as discussed previously. Resulting inferred ambient scattering values are plotted against the altitude at 550 nm (Figure 8e). Total (gray dots), median (circles), and submicron (solid squares) contributions are shown. The scattering coefficient provides many more data points than those obtained from our size distributions but confirms the same features. About 20% of the median total scattering and differential AOD up to 2000 m are due to submicron particles that passed through the 1-μm impactor (dry condition). Note that several altitudes have many data with a

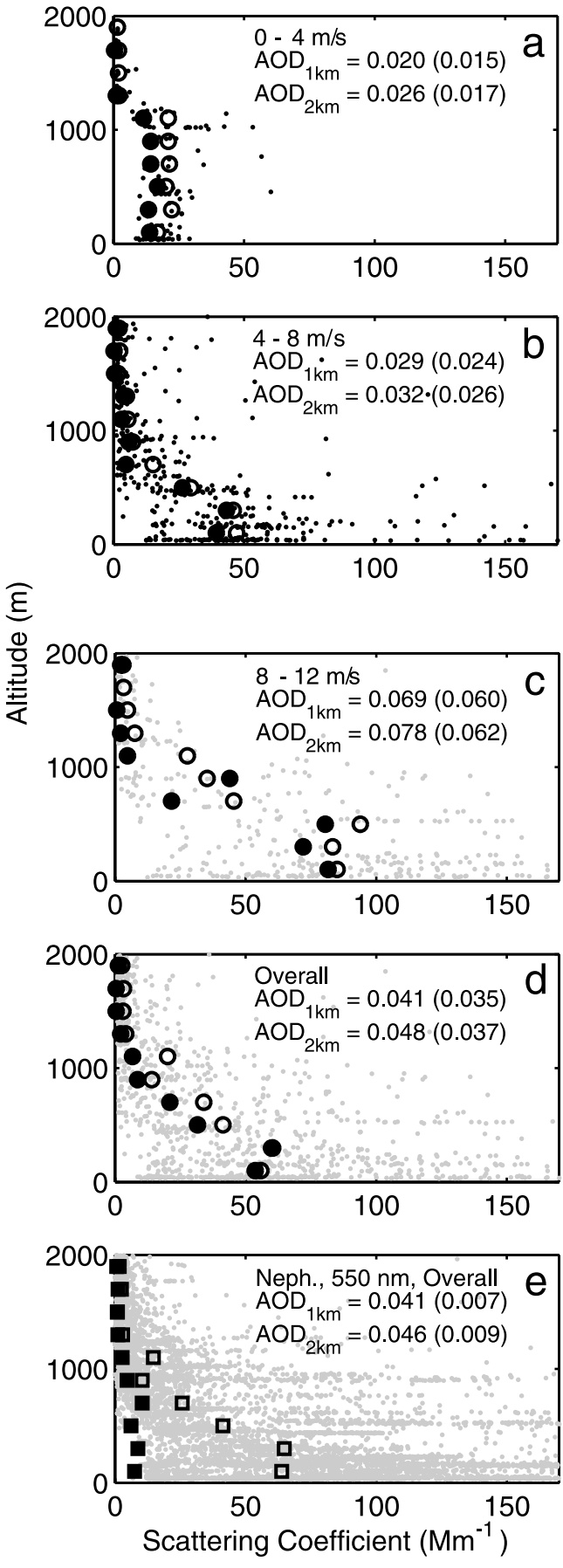

very wide range of the scattering coefficients. This is because several flights under different light scattering conditions flew at common altitudes.

3.3. Column Aerosol Optical Depth

[38] The scattering profiles shown in Figure 8 are statistically and regionally representative and enable us to estimate average AOD over the column. For the contribution from the higher altitudes 2000–5500, we used 0.0040 for ACE 1 and 0.0044 for PEMT-B, which are the integrals of median nephelometer ambient scattering coefficients over this altitude range. If we assume these values scale with pressure (i.e., constant mixing ratio), then multiplication by a scaling factor of 0.58 yields an estimated of the differential AOD over upper troposphere between 6 km and tropopause. For the stratosphere, 0.005 was adopted from previous studies [*Toon and Pollack*, 1976; *Russell et al.*, 1993]. The resulting aircraft-based AOD estimates are listed in Table 2 at 500 nm wavelength. This table also includes the optical depths compared with the Sun photometer optical depth measurements aboard R/V *Discoverer* for the three cases when the aircraft and ship were in close proximity (see section 2.2).

[39] The sources of uncertainties (Table 1) include the stratosphere AOD estimate, free troposphere estimate and mesoscale variability (section 4) in addition to those associated with the OPC measurements and modeling for the MBL. The relative uncertainty in the free troposphere AOD estimate is smaller than that in the MBL ambient scattering estimate because the inlet loss has little impact for the free troposphere aerosols with smaller mean diameters and because the diameter adjustment for ambient RH was not necessary.

4. Spatial Variability

[40] Here we provide a statistical assessment of mesoscale variability in scattering coefficients with altitude. The scattering coefficients plotted in Figure 2 have been averaged over horizontal legs lasting usually 20–30 min. However, significant variation in aerosol properties are present over scales of several to tens of kilometers and contribute to the variability in sea-salt concentration for a given wind speed. This is evident in Figure 9a for the

Figure 8. (a–d) Vertical scattering profiles during the entire ACE 1 flights over the remote Southern Ocean. The OPC-derived total ambient scattering coefficients at 500 nm have been sorted by the 10-m wind speeds and collectively plotted against altitude (gray dots). The open and solid circles are median values in each 200-m altitude bin at 40°C and 300°C, respectively, with the difference due to the volatile component. The differential optical depths up to 1000 m (aerosol optical depth (AOD_{1km})) and 2000 m (AOD_{2km}) are given as the integral of median values for the unheated measurements with the heated measurements in parentheses. (e) Same as Figures 8a–8d except for the use of nephelometer data at 550-nm wavelength. The total and submicron median values are shown with open and solid squares, respectively. The AOD are shown for the total particles with the submicron values in parentheses.

Table 2. Aerosol Optical Depth Estimates and Measurements[a]

Platform/Time	WS, m s^{-1}	Total	$SS_{<2\ km}$	(SN)	$V_{<2\ km}$	(SN)	FT	Stratosphere
				Southern Ocean				
ACE 1 C-130								
1995 average	overall	0.059	0.037	(570)	0.011	(974)	0.006	0.005
(Nov. and Dec.)	0–4	0.037	0.017	(62)	0.009	(125)	0.006	0.005
	4–8	0.043	0.026	(232)	0.006	(462)	0.006	0.005
	8–12	0.090	0.062	(276)	0.017	(387)	0.006	0.005
ACE 1 Discoverer								
1995 flight 17		0.110						
1995 flight 22		0.038						
1995 flight 24		0.066						
				Tropical Pacific Ocean				
PEMT-B P-3B								
1999 average	overall	0.072	0.022	(493)	0.038	(515)	0.007	0.005
(March and April)	3–5	0.060	0.014	(125)	0.034	(127)	0.007	0.005
	5–7	0.062	0.017	(244)	0.033	(253)	0.007	0.005
	7–9	0.128	0.052	(124)	0.064	(135)	0.007	0.005

Platform/Time	Total	Marine Boundary Layer (Height)	$FT_{<5.5\ km}$	$FT_{>5.5\ km}$ Plus Stratosphere
ACE 1 C-130				
1995 flight 17	0.115	0.091 (1.6 km)	0.006	0.018
1995 flight 22	0.046	0.022 (1.4 km)	0.005	0.019
1995 flight 24	0.058	0.021 (0.7 km)	0.020	0.017

Platform/Time	Total	Marine Boundary Layer Plus FT	Stratosphere
Cape Grim			
1986–1999, Nov.	0.053	0.048	0.005
1986–1999, Dec.	0.042	0.037	0.005

[a]Wavelength is 500 nm. Sun photometer was used on Discoverer and Cape Grim. OPC and nephelometer measurements were used for the C-130 and P-3B estimates along with satellite measurements. WS is the 10-m wind speed, AOD is aerosol optical depth, SS is sea salt, V is volatile aerosols, n is OPC sample number, and FT is free troposphere. The Cape Grim data are after *Wilson and Forgan* [2002].

measured nephelometer scattering coefficient during four consecutive horizontal circles (60 km diameter) during ACE 1 flight 19 on 2 December 1995. Scattering varies with latitude and is higher over the southern part of all circles flown at 50, 170, 530 and 920 m altitude.

[41] Clouds associated with frontal activity were observed over the regions to the north of the flight path, and are expected to have scavenged some aerosol in the northern part of the horizontal circles. Low scattering coefficients are also evident at the beginning of the 910-m leg. This is associated with low ambient RH and an increase in potential temperature by 2°–3° (not shown) consistent with passing the inversion into drier free troposphere air with fewer aerosols. The degree of variability is indicated by the coefficient of variance (CV), or standard deviation divided by the mean. The CV for the dry aircraft nephelometer scattering coefficient is 20%, 30%, 45% and 80% for the four horizontal legs. This does not differ significantly from variability in ambient scattering that includes effects of ambient RH variation (i.e., 20%, 30%, 45% and 90%, respectively) for these legs.

[42] Figure 9b shows the CV for the dry nephelometer scattering coefficient for all horizontal legs flown during ACE 1. The wind speed remained within ±2 m s^{-1} of the average over each circle for most of the horizontal legs. The CV remain relatively small in the lower MBL up to 350 m (where most of the dots lie between 0 and 20% in 0–200 m) but increase at higher altitudes. For two thirds of the horizontal legs up to 2000 m, the standard deviation falls between 0.34 and 3.5 Mm^{-1}, and the coefficient of variance lies between 6.9 and 38%. This mesoscale variability is much larger than nephelometer precision of 0.1 Mm^{-1} and exists over times as short as 1 min (Figure 9a) at a normal aircraft speed, equivalent to several kilometers in flight distance. This explains the relationship between the OPC and nephelometer scattering coefficients when they are compared in 2-min interval as opposed to leg average: the R^2 for the 550 nm total closure drops from 0.99 for the leg average closure to 0.92 for the point-to-point closure. When the mean CV over each 200-m-altitude bin is applied to the median scattering profile (circles in Figure 8a), it yields a variability of about 25% in the differential column optical depth up to 2000 m.

[43] Such spatial variability within a 60 km circle may be attributed to several causes other than variable sea-salt production rates. The data in Figure 9a that include the noted variation in cloud cover between north and south are highlighted in the squares in Figure 9b. These have a CV that is about a factor of 2 larger than the ACE 1 mean and suggesting that cloud processes, including scavenging and entrainment, play a significant role in modulating the CV of aerosol concentration on the mesoscale. Hence prior cloud activity on temporal scales shorter than sea-salt residence times could have large impacts on mesoscale variability. This mesoscale variability also needs to be considered in comparing the column optical depth derived from the aircraft in situ measurements with the satellite or surface measurements, because aircraft profiles typically extend over tens of kilometers.

5. Discussion and Conclusions

[44] The ACE 1 and PEMT-B missions provided opportunities to study marine aerosol optical properties under

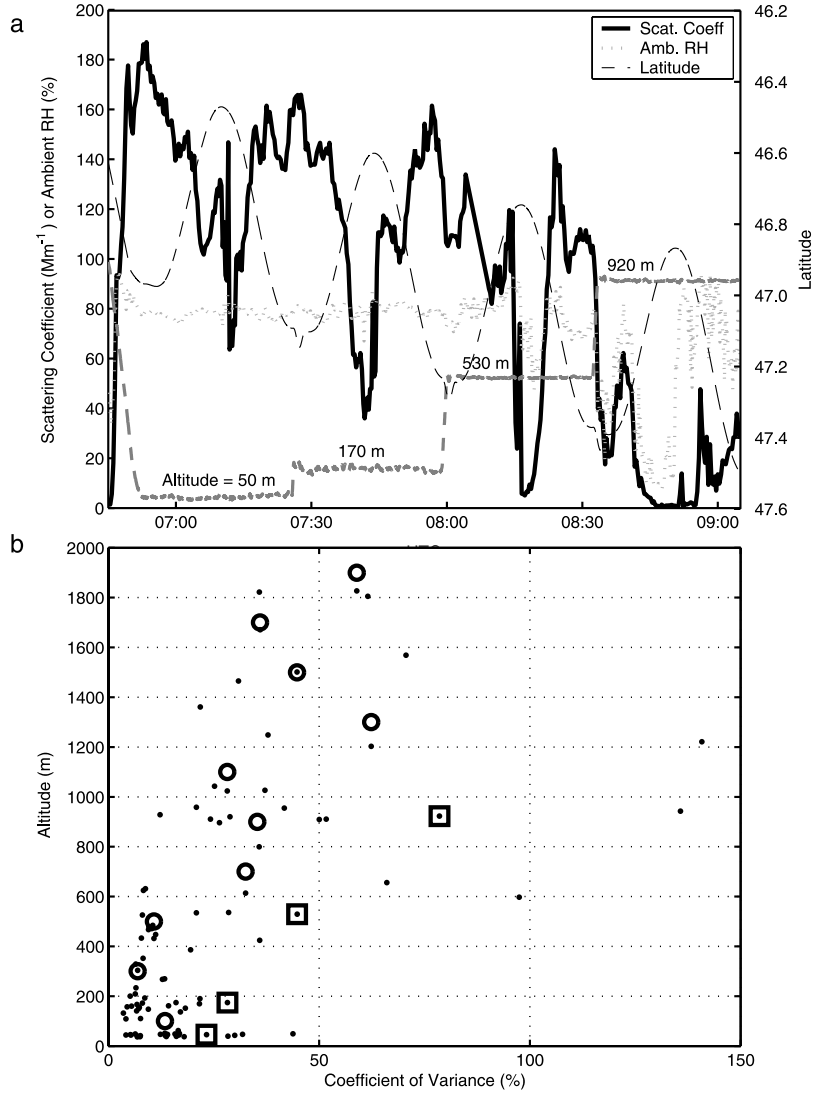

Figure 9. (a) Ambient scattering coefficient during horizontal legs during ACE 1 flight 19 on 2 December 1995. Also shown are ambient relative humidity and latitude. (b) Mesoscale variability in dry airborne nephelometer scattering coefficient. Each dot represents the coefficient of variance within a horizontal leg that lasted at least 20 min. Circles indicate median values in each 200-m-altitude bin. The four squares are for the horizontal legs shown in Figure 9a.

clean atmospheric conditions and to describe their dependence on wind speed. Thermal analysis of particles at near 40°C, 150°C, and 300°C enabled us to estimate size distributions of the volatile (mostly sulfate and possibly organic) and refractory (mostly sea salt) modes as well as their contributions to optical depth. Recent evaluations of the sampling efficiency of the inlets during PELTI have enabled us to implement size-resolved concentrations necessary for the evaluations presented here. Our assumptions and procedures for adjusting the OPC size distribution were evaluated through closure with independent scattering and mass measurements under dry conditions. Resulting local aircraft closure between scattering coefficient under dry conditions derived from the OPC size distributions and the nephelometer scattering coefficient as measured inside the aircraft agreed within 1% (R^2 = 0.97) at 550 nm.

[45] However, we note that an earlier study by *Fridlind and Jacobson* [2003, Figure 2e], identified the OPC-to-nephelometer scattering ratio as 0.73 for the 0°–180° scattering at 550 nm. One explanation for this difference is that they chose only flights 22 and 24, while the present study considered all the 18 flights during ACE 1 over the remote ocean. Data points for these two flights lie near the lower values in the data set in our Figure 2 with our OPC to nephelometer ratio being 0.86 for total scattering. Also, in their assessment the OPC diameters are assumed to be geometric and not converted from optically effective sizes as mentioned in section 2.2 of this study. The OPC diameter adjustment makes at least a 14% difference in scattering. The combination of these two factors lower the slope closer to their value. Other possible minor factors include difference in assumed chemical composition. They used varying refractive indices calculated on the basis of modeled chem-

Table 3. Comparison of Aerosol Components Between ACE 1 and PEMT-B

Property	ACE 1	PEMT-B
	Sea Salt	
Volume	twice as large for ACE 1 as for PEMT-B	twice as large for ACE 1 as for PEMT-B
Scattering[a]	85%	60%
AOD	0.037	0.022
	Volatile Particles	
Number	smaller concentration and neutralization for ACE 1	smaller concentration and neutralization for ACE 1
Scattering[a]	8%	27%
AOD	0.011	0.038
WS[b]	0–12 m s^{-1}	3–9 m s^{-1}
Latitude	40–55°S	5°N–20°S

[a]Relative contribution to total scattering over 0–200 m.
[b]Typical 10-m wind speed.

ical compositions, and this is different from our choice of refractive indices based on the OPC volatility analysis.

[46] *Fridlind and Jacobson* [2003] also show different results of column optical depth closure for two of the three time periods studied here. They used the aircraft OPC data to scale the ship APS size distributions for the vertical variability in particles in each size. Our AOD estimates were made after adjusting the size distributions for the RH growth and adding the contributions by upper troposphere and stratosphere. Their resulting modeled AOD at 500 nm is smaller than our modeled AODs by 0.007 (14%) and 0.005 (8%) for flights 22 and 24, respectively. This probably results from the same reasons mentioned above.

[47] Profiles of size distributions with the thermal analysis resolved volatile and refractory contributions over stepped layers at selected altitudes. The average distributions show positive dependency of the refractory sea-salt concentration on wind speed for the coarse mode. The volatile component did not show a dependency on wind speed. Consequently, the fractional contributions to number and scattering by the aerosol components vary considerably with wind speed. In the accumulation mode present below 200 m during ACE 1, about 26% of the particle number is sea salt, and this fraction increases with wind speed: 11% (0–4 m s^{-1}), 20% (4–8 m s^{-1}) and 31% (8–12 m s^{-1}).

[48] This suggests that the number of cloud condensation nuclei (CCN) in the MBL is certainly affected by this variation in sea-salt fraction of submicron particles. Assuming that all particles larger than 0.15 μm act as CCN, we estimate that about 20% of these are sea salt under wind speeds higher than 8 m s^{-1} during ACE-1, while the ratio would be less than 10% under 4 m s^{-1}. The smaller number fraction of sea salt lowers its relative importance as CCN during PEMT-B. In any event, global climate models that consider only sulfate CCN would underestimate the number of CCN and hence the cloud coverage and cooling effect.

[49] Sea salt is the major contributor to ambient scattering and contributes 96% over 0–200 m in the ACE 1 (Figure 8a). The scattering coefficients under dry condition drops to 87%, and this is only slightly smaller than the ACE 1 near-surface (~30 m) ship measurements where more than 95% of the scattering is due to sea salt under 30–40% RH [*Quinn and Coffman*, 1999].

[50] The ACE 1 (Figure 6) and PEMT-B (Figure 7) size distributions show distinctive differences in coarse-mode sea salt and accumulation volatile particles, as summarized in Table 3. The PEMT-B coarse-mode sea-salt volume is <50% of that in ACE 1. This is likely a result of weaker production from lower winds. In contrast, the volatile accumulation particles have larger concentration and larger fraction of neutralized components in PEMT-B than in ACE 1. The high concentrations of neutralized aerosol over the tropical region may be associated with a longer residence time due to weak precipitation scavenging and stronger sources of dimethyl sulfide and photochemical production of sulfur dioxide [*Bandy et al.*, 1996] leading to aerosol sulfate [*Huebert et al.*, 1996]. Weaker removal and a strong surface ammonia flux can lead to a high degree of neutralization in this region [*Clarke and Porter*, 1993]. As a result, relative contributions of sea salt to total scattering is smaller, and that of volatile particles larger, in PEMT-B compared to ACE 1.

[51] The observed wind speed dependence of column AOD is summarized in Figure 10 and Table 2. Sea-salt contribution relative to the total column AOD is larger over the Southern Ocean (63%) than over the Tropical Pacific Ocean (31%). The lower sea-salt contribution to AOD for wind speeds below ~7 m s^{-1} in the tropics compared to midlatitudes may reflect the lower frequency of higher winds occurring in the tropics. As a result, the less frequent generation can be expected to lead to lower average concentrations for a given wind speed in the tropics. On the other hand, the MBL AOD (sum of contributions from volatile particles and sea salt) and the total column AOD are larger over the tropical region because of a greater contribution of volatile particles as discussed above. Both campaigns reveal a sudden rise in the average AOD for 10-m wind speeds above 7–8 m s^{-1}. The right panel of Figure 10 includes a comparison to total column aerosol optical depth observed from ground measurements on Midway Island [*Smirnov*, 2003]. Although a low R^2 value of 0.14 is associated with their regression line, indicating a large variance in AOD at a given wind speed, the slopes of the wind speed dependence is similar to ours. Although the slope is driven by variation in wind speed, the large contribution from volatile aerosol to AOD may help explain their observed low R^2. Our altitude-resolved AOD and the column-integral observation agree within the observed variance.

[52] It is also of interest to compare our average results to typical optical depths measured at the surface near the ACE 1 study region during the same months. *Wilson and Forgan* [2002] report optical depth measurements made at Cape Grim, Tasmania (90 m altitude), for the period 1986–1999 (except for the year 1991 right after the Mount Pinatubo eruption). Their 500-nm optical depths averaged over November and December are 0.048 and 0.037, respectively. Note that the average estimated contribution from the stratospheric aerosol for this time period was removed from this literature value. If we add 0.005 as the contribution from the lowest 90 m for an assumed scattering coefficients of 50 Mm^{-1}, our ACE 1 aircraft-based

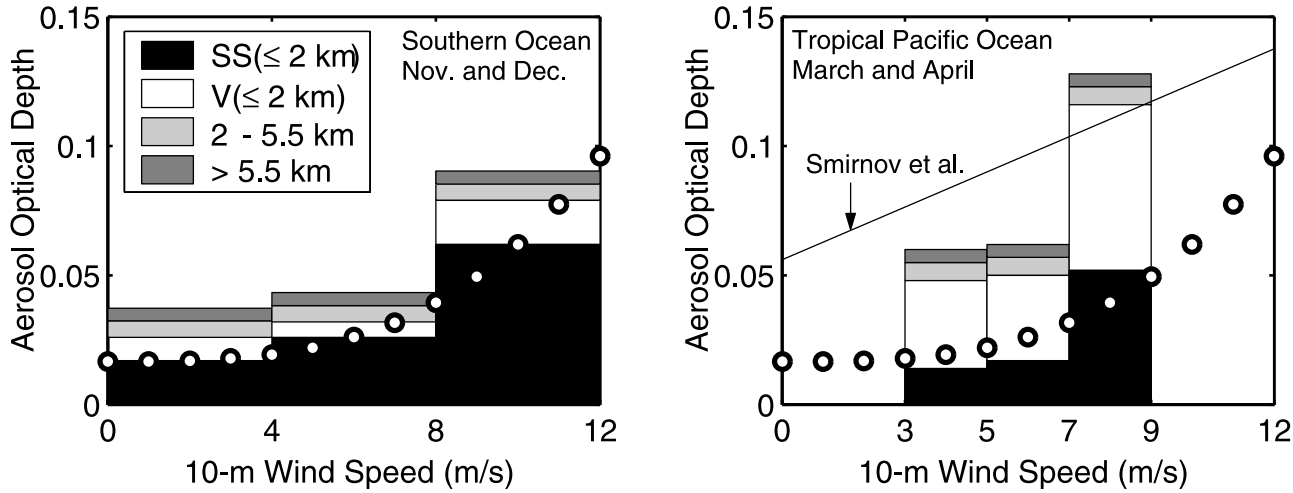

Figure 10. Aerosol optical depth averaged over (left) ACE 1 and (right) PEMT-B observations for the 10-m wind speed categories. The legend reads (from top) sea salt (SS) over 0–2 km, volatile particles (V) over 0–2 km, total aerosols over 2–5.5 km, and total aerosols over 5.5 km to top of atmosphere. See Table 2 for the individual differential AOD values and sample numbers. The circles indicate approximated expressions to ACE 1 sea-salt AOD. Mean AOD (500 nm) observed at Midway Island by AERONET is also plotted in the right panel against surface wind speed averaged within 24 hours prior the instantaneous AOD measurement [*Smirnov et al.*, 2003].

AOD estimate (Figure 10) is well within the observed variance of their value.

[53] The relative importance of the MBL in the total mean column AOD can be identified for the 10-m wind speed categories. For the average data (Figure 8), we consider the differential contribution of <2000-m layer as the MBL AOD because the inversion height varies from several hundred meters to 2 km. Using differential AOD from 2 km to the top of atmosphere shown in the previous section, the relative fraction of total column AOD contributed by the MBL during ACE 1 averages 81% under ambient conditions. This fraction is 70% for winds of 0–4 m s^{-1}, 74% under 4–8 m s^{-1} and 88% under 8–12 m s^{-1}. For PEMT-B, the ambient MBL median differential AOD comprises 83% of the total AOD collectively, or 80%, 81% and 91% under 10-m wind speeds of 3–5, 5–7 and 7–9 m s^{-1}, respectively. Thus, in spite of the distinctive difference in relative contributions of sea salt and volatile particles within the MBL, the MBL contribution to the column AOD remains similar between the two regions.

[54] Sea-salt contribution to optical depth for ACE 1 can be approximated by

$$\mathrm{AOD(SS)} = 4.9 \times 10^{-5} w^3 - 3.7 \times 10^{-5} w^2 + 0.017 \quad (1)$$

where w is 10-m wind speed (m s^{-1}). There is no significant difference in the wind speed dependency of sea-salt concentration between the two locations, while the mean sea-salt concentration is somewhat lower over the tropical Pacific Ocean because of lower mean wind speed compared to the conditions over the Southern Ocean. It should be kept in mind that these expressions reflect the combined effects of both the generation and the removal processes on the limited number of samples for the field studies in these regions.

[55] We have also characterized the horizontal mesoscale variability in MBL scattering coefficient during ACE 1 as 25% on average over scales of 60 km, and this value is smaller at lower altitude. Cloud processing, fetch, and vertical mixing can affect this variability. As a consequence, a column AOD obtained from a single vertical profile in the ACE 1 region has been shown to have a 25% uncertainty relative to the mesoscale average. Analogous to the calculated standard deviation, we assume that the length of error bar associated with the mean AOD is proportional to the reciprocal of square root of number of vertical profiles. Then, two profiles would reduce the error bar to 18% ($25\%/2^{1/2}$). Three profiles would reduce the error to 14% ($23\%/3^{1/2}$). Hence an average of three profiles in this region would be needed for AOD comparisons or closure if the influence of mesoscale variability on AOD measurements is to be less than 15%.

[56] In summary, a quantitative dependence of AOD and wind speed was present in both tropical and midlatitude data that was due to sea salt. However, this is only evident when averaging over significant spatial or temporal scales because of mesoscale variability in the aerosol fields. Consequently, satellite retrievals of aerosol properties such as AOD and in situ vertical profiles as well as ground measurements should be averaged over appropriate scales for realistic comparisons (e.g., "closure").

[57] **Acknowledgments.** This analysis was supported by the Office of Naval Research N00014-96-1-0320 on data collected under NSF ATM-9419475, NASA NCC-1-315 and NASA NAGW3766. We are grateful for the nephelometer sensitivity data provided by Tad Anderson. Yohei Shinozuka thanks the Rotary Foundation, the Crown Prince Akihito Scholarship Foundation and the University of Hawaii Foundation for partial funding support.

References

Anderson, T. L., et al. (1996), Performance characteristics of a high-sensitivity, three-wavelength, total scatter/backscatter nephelometer, *J. Atmos. Oceanic Technol.*, *13*, 967–986.

Andreas, E. L. (1998), A new sea spray generation function for wind speed up to 32 m s^{-1}, *J. Phys. Oceanogr.*, *28*, 2175–2184.

Bandy, A. R., D. C. Thornton, B. W. Blomquist, S. Chen, T. P. Wade, J. C. Ianni, G. M. Mitchell, and W. Nadler (1996), Chemistry of dimethyl sulfide in the equatorial Pacific atmosphere, *Geophys. Res. Lett.*, *23*(7), 741–744.

Bates, T. S., B. J. Huebert, J. L. Gras, F. B. Griffiths, and P. A. Durkee (1998a), International Global Atmospheric Chemistry (IGAC) Project's First Aerosol Characterization Experiment (ACE 1): Overview, *J. Geophys. Res.*, *103*(D13), 16,297–16,318.

Bates, T. S., V. N. Kapustin, P. K. Quinn, D. S. Covert, D. J. Coffman, C. Mari, P. A. Durkee, W. J. D. Bruyn, and E. S. Saltzman (1998b), Processes controlling the distribution of aerosol particles in the lower marine boundary layer during the First Aerosol Characterization Experiment (ACE 1), *J. Geophys. Res.*, *103*(D13), 16,369–16,383.

Bates, T. S., P. K. Quinn, D. J. Coffman, J. E. Johnson, T. L. Miller, D. S. Covert, A. Wiedensohler, S. Leinert, A. Nowak, and C. Neususs (2001), Regional physical and chemical properties of the marine boundary layer aerosol across the Atlantic during Aerosols99: An overview, *J. Geophys. Res.*, *106*(D18), 20,767–20,782.

Blanchard, D. C., and A. H. Woodcock (1957), Bubble formation and modification in the sea and its meteorological significance, *Tellus*, *9*, 145–158.

Blanchard, D. C., and A. H. Woodcock (1980), The production, concentration, and vertical distribution of the sea-salt aerosol, *Ann. N. Y. Acad. Sci.*, *338*, 330–347.

Blomquist, B. W., B. J. Huebert, S. G. Howell, M. R. Litchy, C. H. Twohy, A. Schanot, D. Baumgardner, B. Lafleur, R. Seebaugh, and M. L. Laucks (2001), An evaluation of the Community Aerosol Inlet for the NCAR C-130 research aircraft, *J. Atmos. Oceanic Technol.*, *18*, 1387–1397.

Charlson, R. J., J. E. Lovelock, M. O. Andreae, and S. G. Warren (1987), Oceanic phytoplankton, atmospheric sulfur, cloud albedo and climate, *Nature*, *326*, 655–661.

Clarke, A. D. (1991), A thermo-optic technique for in situ analysis of size-resolved aerosol physicochemistry, *Atmos. Environ., Part A*, *25*, 635–644.

Clarke, A. D., and J. N. Porter (1993), Pacific marine aerosol: 2. Equatorial gradients in chlorophyll, ammonium, and excess sulfate during SAGA 3, *J. Geophys. Res.*, *98*(D9), 16,997–17,010.

Clarke, A. D., T. Uehara, and J. N. Porter (1996), Lagrangian evolution of an aerosol column during the Atlantic Stratocumulus Transition Experiment, *J. Geophys. Res.*, *101*(D2), 4351–4362.

Clarke, A. D., et al. (1998a), Particle nucleation in the tropical boundary layer and its coupling to marine sulfur sources, *Science*, *282*, 89–92.

Clarke, A. D., J. L. Varner, F. Eisele, R. L. Mauldin, D. Tanner, and M. Litchy (1998b), Particle production in the remote marine atmosphere: Cloud outflow and subsidence during ACE 1, *J. Geophys. Res.*, *103*(D13), 16,397–16,409.

Clarke, A. D., W. G. Collins, P. J. Rasch, V. N. Kapustin, K. Moore, S. Howell, and H. E. Fuelberg (2001), Dust and pollution transport on global scales: Aerosol measurements and model predictions, *J. Geophys. Res.*, *106*(D23), 32,555–32,569.

Covert, D. S., V. N. Kapustin, P. K. Quinn, and T. S. Bates (1992), New particle formation in the marine boundary layer, *J. Geophys. Res.*, *97*(D18), 20,581–20,589.

Fridlind, A. M., and M. Z. Jacobson (2003), Point and column aerosol radiative closure during ACE 1: Effects of particle shape and size, *J. Geophys. Res.*, *108*(D3), 4094, doi:10.1029/2001JD001553.

Fuelberg, H. E., R. E. Newell, D. J. Westberg, J. C. Maloney, J. R. Hannan, B. D. Martin, M. A. Avery, and Y. Zhu (2001), A meteorological overview of the second Pacific Exploratory Mission in the tropics, *J. Geophys. Res.*, *106*(D23), 32,427–32,443.

Hegg, D. A., D. S. Covert, and V. N. Kapustin (1992), Modeling a case of particle nucleation in the marine boundary layer, *J. Geophys. Res.*, *97*(D9), 9851–9857.

Hoppel, W. A., J. W. Fitzgerald, G. M. Frick, R. E. Larson, and E. J. Mack (1990), Aerosol size distributions and optical properties found in the marine boundary layer over the Atlantic Ocean, *J. Geophys. Res.*, *95*(D4), 3659–3686.

Huebert, B. J., G. Lee, and W. L. Warren (1990), Airborne aerosol inlet passing efficiency measurement, *J. Geophys. Res.*, *95*(D10), 16,369–16,381.

Huebert, B. J., D. J. Wylie, L. Zhuang, and J. A. Heath (1996), Production and loss of methanesulfonate and non-sea salt sulfate in the equatorial Pacific marine boundary layer, *Geophys. Res. Lett.*, *23*(7), 737–740.

Huebert, B. J., S. G. Howell, L. Zhuang, J. A. Heath, M. R. Litchy, D. J. Wylie, J. L. Kreidler-Moss, S. Coppicus, and J. E. Pfeiffer (1998), Filter and impactor measurements of anions and cations during the First Aerosol Characterization Experiment (ACE 1), *J. Geophys. Res.*, *103*(D13), 16,493–16,509.

Huebert, B. J., et al. (2004), PELTI: Measuring the passing efficiency of an airborne low turbulence aerosol inlet, *Aerosol Sci. Technol.*, *38*, 803–826.

Kalashnikova, O. V., and I. N. Sokolik (2002), Importance of shapes and compositions of wind-blown dust particles for remote sensing at solar wavelengths, *Geophys. Res. Lett.*, *29*(10), 1398, doi:10.1029/2002GL014947.

Koponen, I. K., A. Virkkula, R. Hillamo, V.-M. Kerminen, and M. Kulmala (2002), Number size distributions and concentrations of marine aerosols: Observations during a cruise between the English Channel and the coast of Antarctica, *J. Geophys. Res.*, *107*(D24), 4753, doi:10.1029/2002JD002533.

Large, W. G., and S. Pond (1981), Open ocean momentum flux measurements in moderate to strong winds, *J. Phys. Oceanogr.*, *11*, 324–336.

Lovett, R. F. (1978), Quantitative measurement of airborne sea-salt in the North Atlantic, *Tellus*, *30*, 358–364.

Maring, H., D. L. Savioe, M. A. Izaguirre, L. Custals, and J. S. Reid (2003), Vertical distributions of dust and sea-salt aerosols over Puerto Rico during PRIDE measured from a light aircraft, *J. Geophys. Res.*, *108*(D19), 8587, doi:10.1029/2002JD002544.

McInnes, L. M., D. S. Covert, P. K. Quinn, and M. S. Germani (1994), Measurement of chloride depletion and sulfur enrichment in individual sea-salt particles collected from the remote marine boundary layer, *J. Geophys. Res.*, *99*(D4), 8257–8268.

Mishchenko, M. I., L. D. Travis, R. A. Kahn, and R. A. West (1997), Modeling phase functions for dustlike tropospheric aerosols using a shape mixture of randomly oriented polydisperse spheroids, *J. Geophys. Res.*, *102*(D14), 16,831–16,847.

Nilsson, E. D., U. Rannik, E. Swietlicki, C. Leck, P. P. Aalto, J. Zhou, and M. Norman (2001), Turbulent aerosol fluxes over the Arctic Ocean: 2, Wind-driven sources from the sea, *J. Geophys. Res.*, *106*(D23), 32,139–32,154.

O'Dowd, C. D., and M. H. Smith (1993), Physicochemical properties of aerosols over the northeast Atlantic: Evidence for wind-speed-related submicron sea-salt aerosol production, *J. Geophys. Res.*, *98*(D1), 1137–1149.

O'Dowd, C. D., et al. (2002), Coastal new particle formation: Environmental conditions and aerosol physicochemical characteristics during nucleation bursts, *J. Geophys. Res.*, *107*(D19), 8107, doi:10.1029/2000JD000206.

Paulson, C. A. (1970), The mathematical representation of wind speed and temperature profiles in the unstable atmospheric surface layer, *J. Appl. Meteorol.*, *9*, 857–861.

Pinnick, R. G., J. D. Pendleton, and G. Videen (2000), Response characteristics of the particle measuring systems active scattering aerosol spectrometer probes, *Aerosol Sci. Technol.*, *33*, 334–352.

Pirjola, L., C. D. O'Dowd, I. M. Brooks, and M. Kulmala (2000), Can new particle formation occur in the clean marine boundary layer?, *J. Geophys. Res.*, *105*(D21), 26,531–26,546.

Porter, J. N., and A. D. Clarke (1997), Aerosol size distribution models based on in situ measurements, *J. Geophys. Res.*, *102*(D5), 6035–6045.

Porter, J. N., M. Miller, C. Pietras, and C. Motell (2001), Ship-based Sun photometer measurements using microtops Sun photometers, *J. Atmos. Oceanic Technol.*, *18*, 765–774.

Potukuchi, S., and A. S. Wexler (1995), Identifying solid-aqueous phase transitions in atmospheric aerosols-I. Neutral-acidity solutions, *Atmos. Environ.*, *29*(14), 1663–1676.

Quinn, P. K., and D. J. Coffman (1999), Comment on "Contribution of different aerosol species to the global aerosol extinction optical thickness: Estimates from model results" by Tegen et al., *J. Geophys. Res.*, *104*(D4), 4241–4248.

Quinn, P. K., D. J. Coffman, T. S. Bates, T. L. Miller, J. E. Johnson, K. Voss, E. J. Welton, and C. Neususs (2001), Dominant aerosol chemical components and their contribution to extinction during the Aerosols99 cruise across the Atlantic, *J. Geophys. Res.*, *106*(D18), 20,783–20,809.

Redemann, J., S. J. Masonis, B. Schmid, T. L. Anderson, P. B. Russell, J. M. Livingston, O. Dubovik, and A. D. Clarke (2003), Clear-column closure studies of aerosols and water vapor aboard the NCAR C-130 during ACE-Asia, 2001, *J. Geophys. Res.*, *108*(D23), 8655, doi:10.1029/2003JD003442.

Reid, J. S., et al. (2003), Comparison of size and morphological measurements of coarse mode dust particles from Africa, *J. Geophys. Res.*, *108*(D19), 8593, doi:10.1029/2002JD002485.

Russell, P. B., et al. (1993), Pinatubo and pre-Pinatubo optical depth spectra: Mauna Loa measurements, comparison, inferred particle size distributions, radiative effects, and relationship to lidar data, *J. Geophys. Res.*, *98*(D12), 22,969–22,985.

Smirnov, A., B. N. Holben, T. F. Eck, O. Dubovik, and I. Slutsker (2003), Effect of wind speed on columnar aerosol optical properties at Midway Island, *J. Geophys. Res.*, *108*(D24), 4802, doi:10.1029/2003JD003879.

Swietlicki, E., et al. (2000), Hygroscopic properties of aerosol particles in the northeastern Atlantic during ACE-2, *Tellus, Ser. B*, *52*, 201–227.

Tang, I. N. (1997), Thermodynamic and optical properties of mixed-salt aerosols of atmospheric importance, *J. Geophys. Res.*, *102*(D2), 1883–1893.

Tang, I. N., A. C. Tridico, and K. H. Fung (1997), Thermodynamic and optical properties of sea salt aerosols, *J. Geophys. Res.*, *102*(D19), 23,269–23,275.

Toon, O. B., and J. B. Pollack (1976), A global average model of atmospheric aerosols for radiative transfer calculations, *J. Appl. Meteorol.*, *15*(3), 225–246.

Twomey, S. (1977), *Atmospheric Aerosols*, 302 pp., Elsevier Sci., New York.

Weber, R. J., P. H. McMurry, L. Mauldin, D. J. Tanner, F. L. Eisele, F. J. Brechtel, S. M. Kreidenweis, G. L. Kok, R. D. Schillawski, and D. Baumgardner (1998), A study of new particle formation and growth involving biogenic and trace gas species measured during ACE 1, *J. Geophys. Res.*, *103*(D13), 16,385–16,396.

Weber, R. J., K. Moore, V. Kapustin, A. Clarke, R. L. Mauldin, E. Kosciuch, C. Cantrell, F. Eisele, B. Anderson, and L. Thornhill (2001), Nucleation in the equatorial Pacific during PEM-Tropics B: Enhanced boundary layer H_2SO_4 with no particle production, *J. Geophys. Res.*, *106*(D23), 32,767–32,776.

Wilson, S. R., and B. W. Forgan (2002), Aerosol optical depth at Cape Grim, Tasmania, 1986–1999, *J. Geophys. Res.*, *107*(D8), 4068, doi:10.1029/2001JD000398.

Woodcock, A. H. (1953), Salt nuclei in marine air as a function of altitude and wind force, *J. Meteorol.*, *10*, 362–371.

Wu, J. (1982), Wind-stress coefficients over sea surface from breeze to hurricane, *J. Geophys. Res.*, *87*(C12), 9704–9706.

A. D. Clarke, S. G. Howell, B. J. Huebert, V. N. Kapustin, and Y. Shinozuka, Department of Oceanography, University of Hawaii at Manoa, 100 Pope Road, Honolulu, HI 96822, USA. (yohei@hawaii.edu)